# Supplementary for "First-principles predictions of the diversity in atomic structures and electronic properties of the reconstructed Si(111)-7×7 surface"

**Table S1.** The summarize of the numbers for dangling bonds (ad-DB, s-DB, iL-DB and Tot-DB) and pairs of dimerization (POD) in different models, as well as the coverage rate ($R_c$) for different reconstructions in Si(111) surface.

| Systems | ad-DB | s-DB | iL-DB | tot-DB | POD | $R_c$ | $N_H$ | $N_{Si}$ | $N_{tot}$ |
|---|---|---|---|---|---|---|---|---|---|
| DAS-3×3 | 2 | 0 | 1 | **3** | 3 | 4/9 | 9 | 70 | 79 |
| DAS-5×5 | 6 | 2 | 1 | **9** | 6 | 6/25 | 25 | 200 | 225 |
| DAS-$d_8$-$T^{12}$ | 12 | 6 | 1 | **19** | 9 | 12/49 | 49 | 394 | 443 |
| DAS-$d_8$-$T^9H^{3\text{-}B}$ | 12 | 6 | 1 | **19** | 9 | 12/49 | 49 | 394 | 443 |
| DAS-$d_8$-$T^9H^{3\text{-}A}$ | 12 | 6 | 1 | **19** | 9 | 12/49 | 49 | 394 | 443 |
| DAS-$d_8$-$T^6H^6$ | 12 | 6 | 1 | **19** | 9 | 12/49 | 49 | 394 | 443 |
| AB-$d_{10}$-$T^{12}$ | 12 | 4 | 1 | **17** | 12 | 12/49 | 49 | 396 | 445 |
| AB-$d_{10}$-$T^9H^3$ | 12 | 4 | 1 | **17** | 12 | 12/49 | 49 | 396 | 445 |
| AA-$d_{10}$-$T^{12}$ | 12 | 4 | 1 | **17** | 12 | 12/49 | 49 | 396 | 445 |
| AA-$d_{10}$-$T^9H^3$ | 12 | 4 | 1 | **17** | 12 | 12/49 | 49 | 396 | 445 |

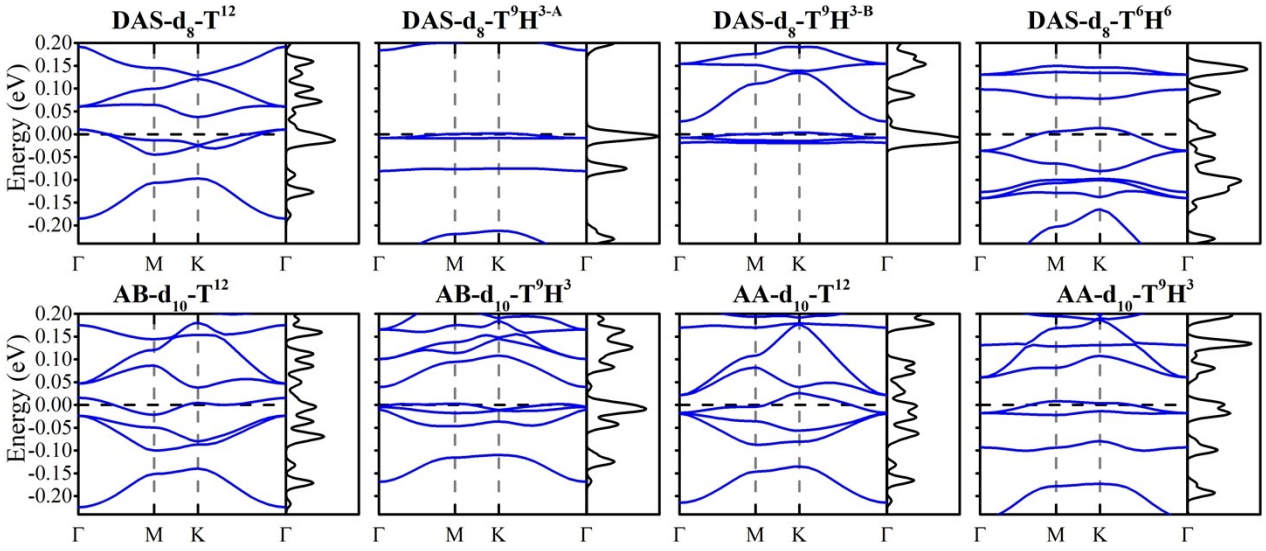


**Fig. S1.** The band structures and density of states of various low-energy Si(111)-7×7 reconstructions calculated in NM states based on PBE functional.

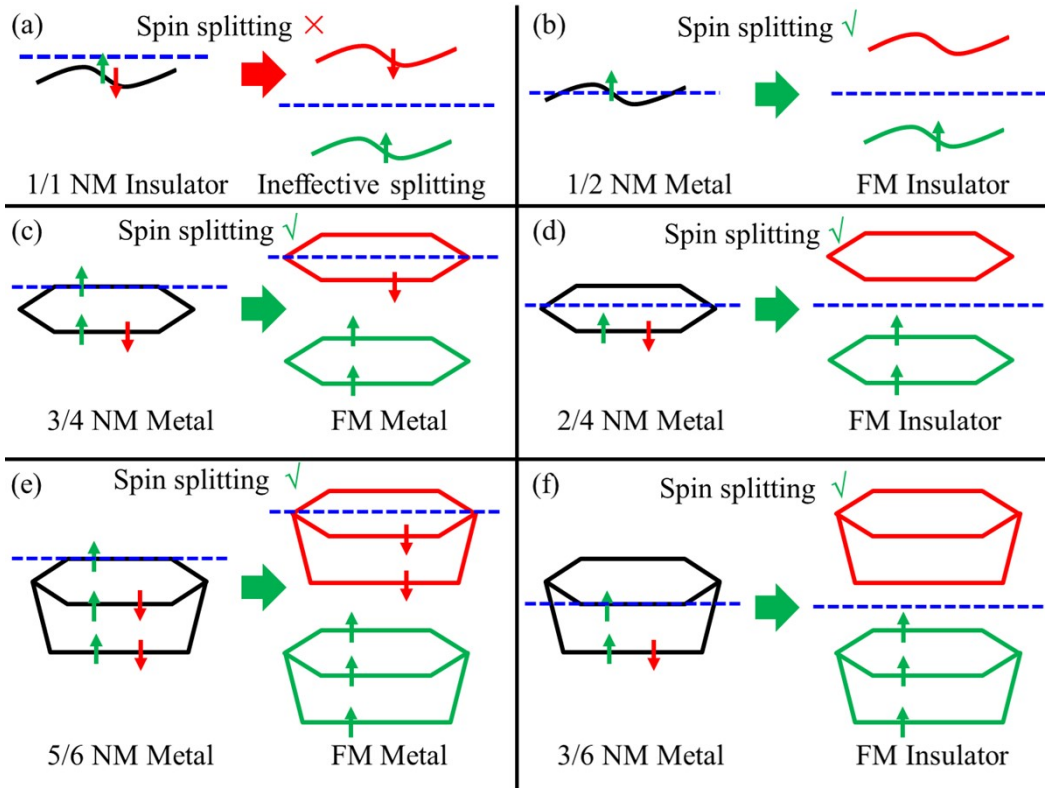


**Fig. S2.** Schematic illustration of spin splitting in isolated narrow-band sets under different filling conditions. Colored solid lines represent energy bands (black for non-spin-polarized, red and green for spin-up and spin-down, respectively). The blue dashed line indicates the Fermi-level, and the up/down arrows represent electron occupancy.

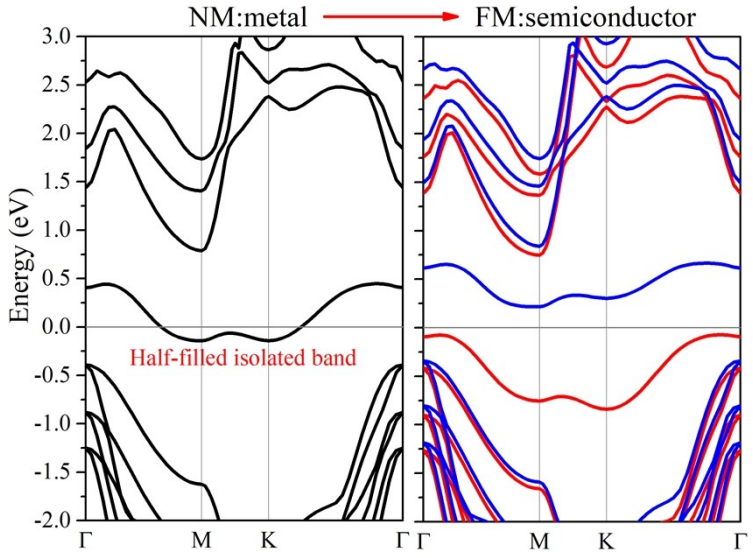


**Fig. S3.** Band structures of the clean Si(111) surface under different magnetic states

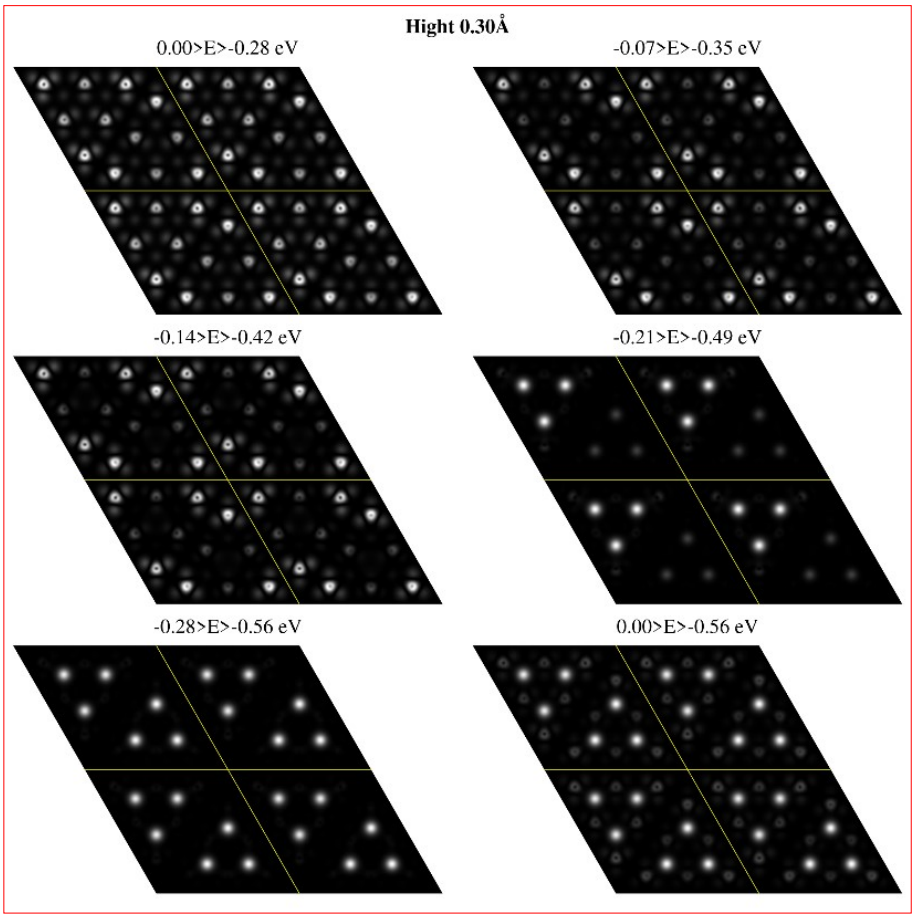


**Fig. S4.** STM of DAS-d8-T12 at the height of 0.3 Å

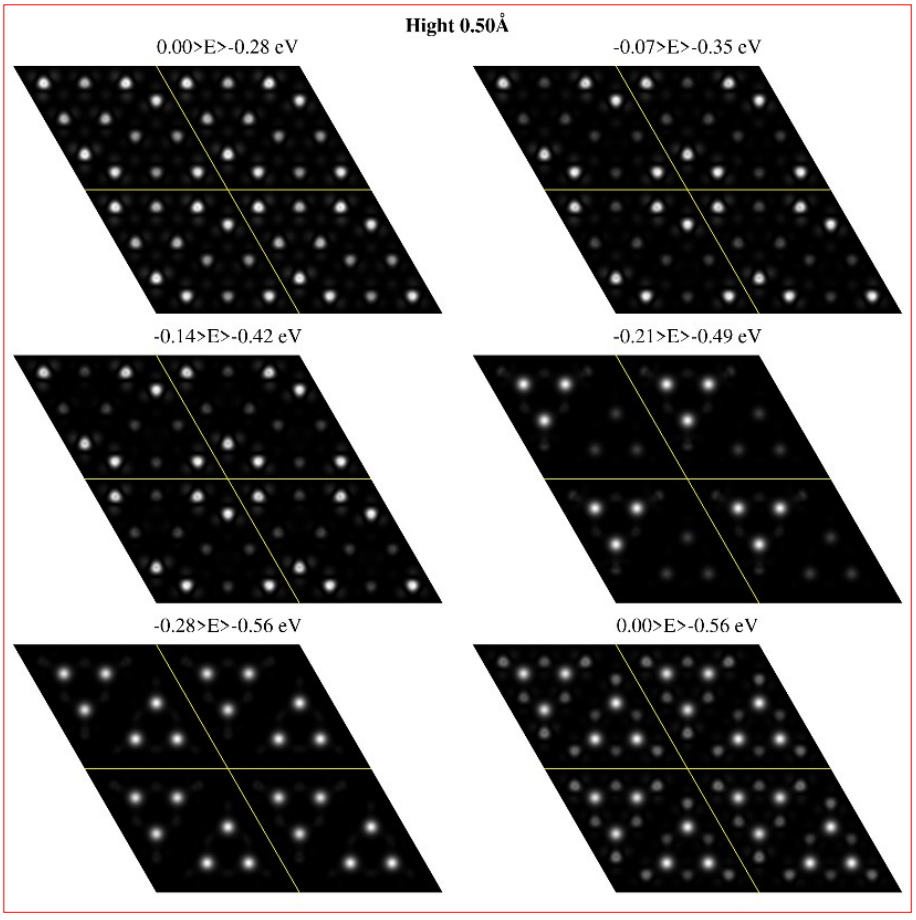


**Fig. S5.** STM of DAS-d8-T12 at the height of 0.5 Å

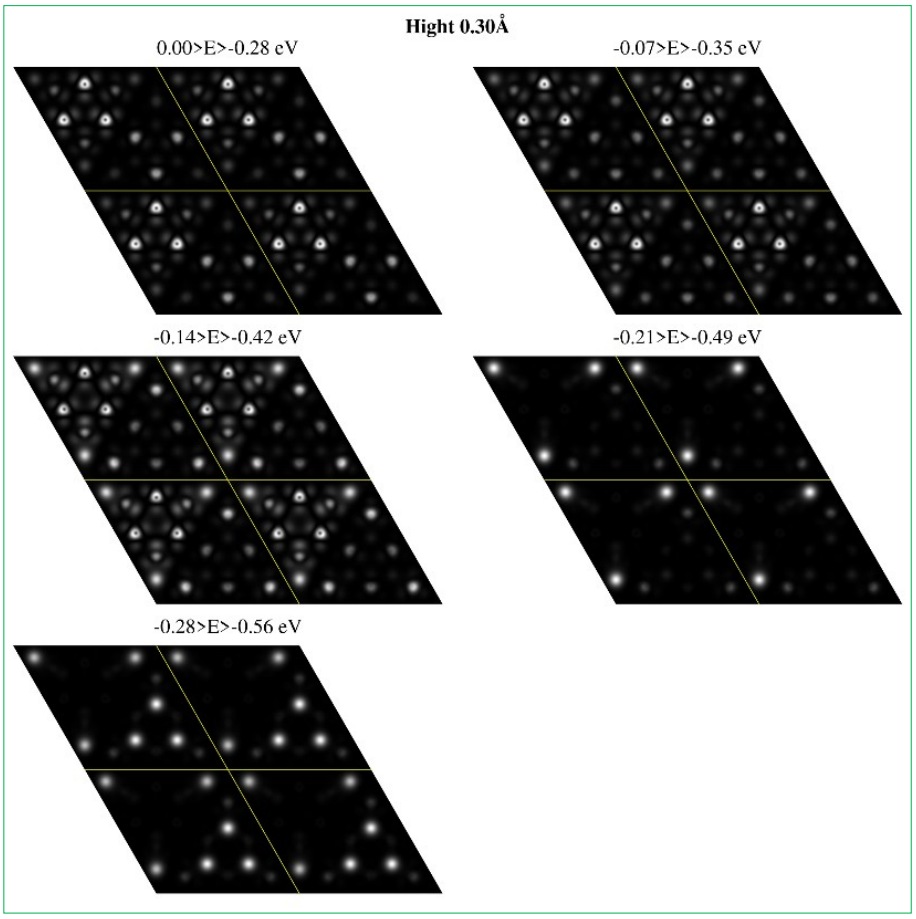


**Fig. S6.** STM of DAS-d8-T9H3-A at the height of 0.3 Å

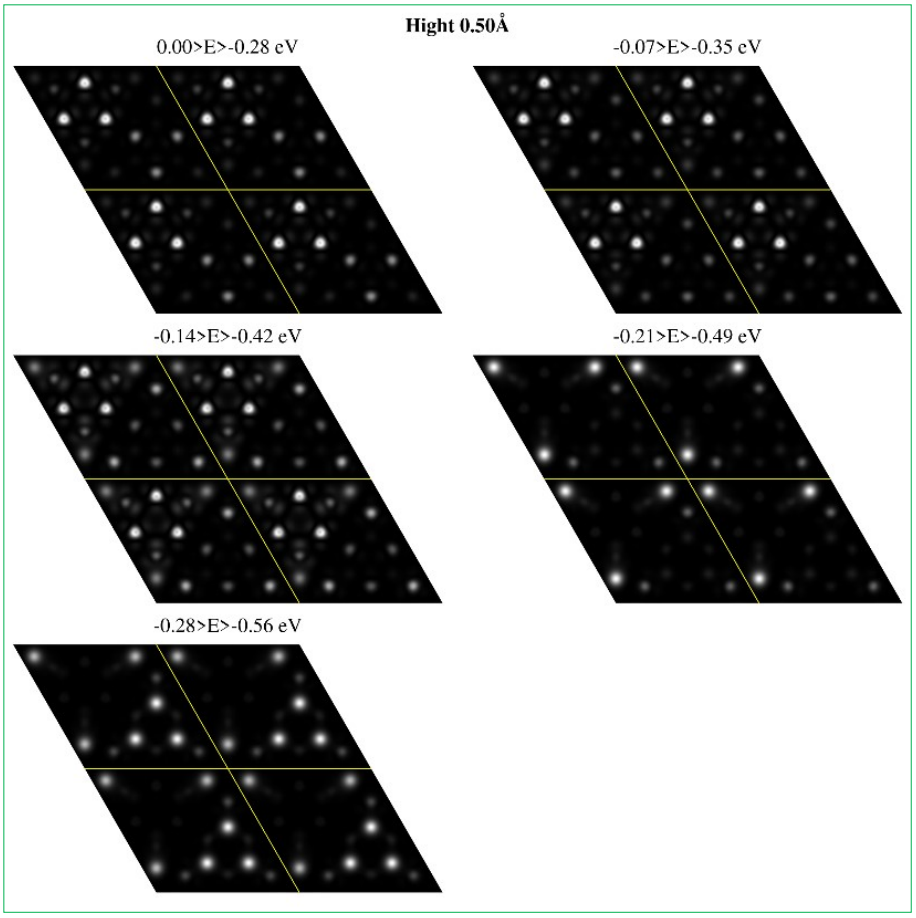


**Fig. S7.** STM of DAS-d8-T9H3-A at the height of 0.5 Å

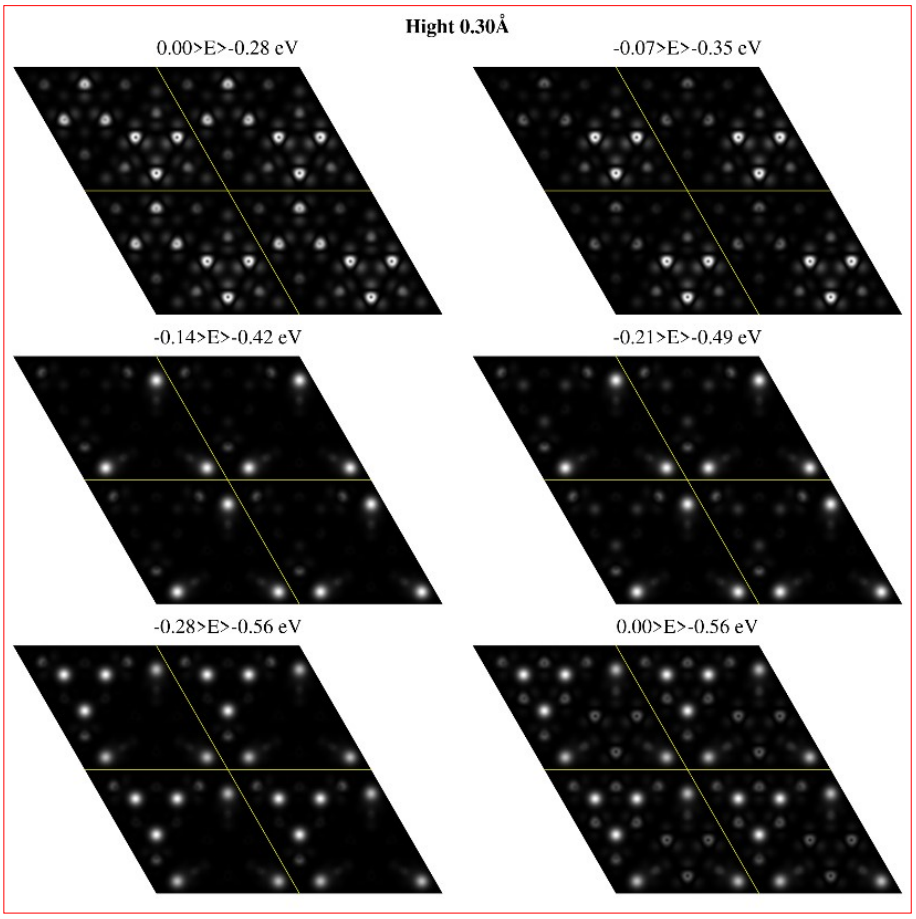


**Fig. S8.** STM of DAS-d8-T9H3-B at the height of 0.3 Å

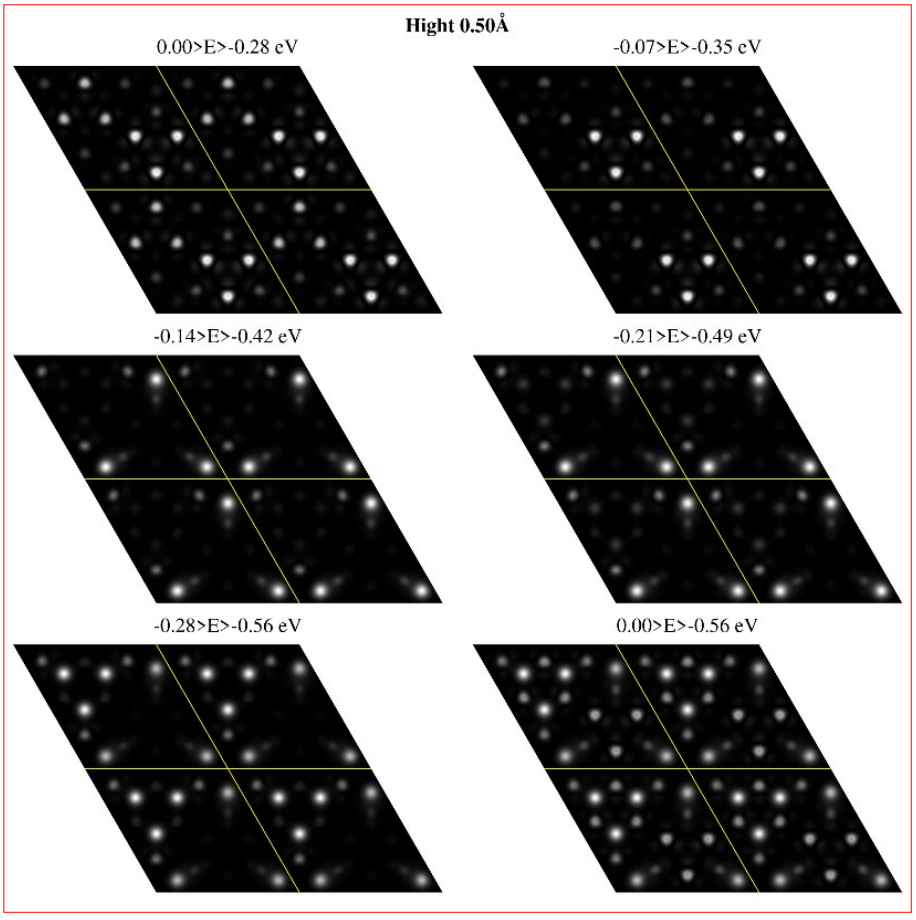


**Fig. S9.** STM of DAS-d8-T9H3-B at the height of 0.5 Å

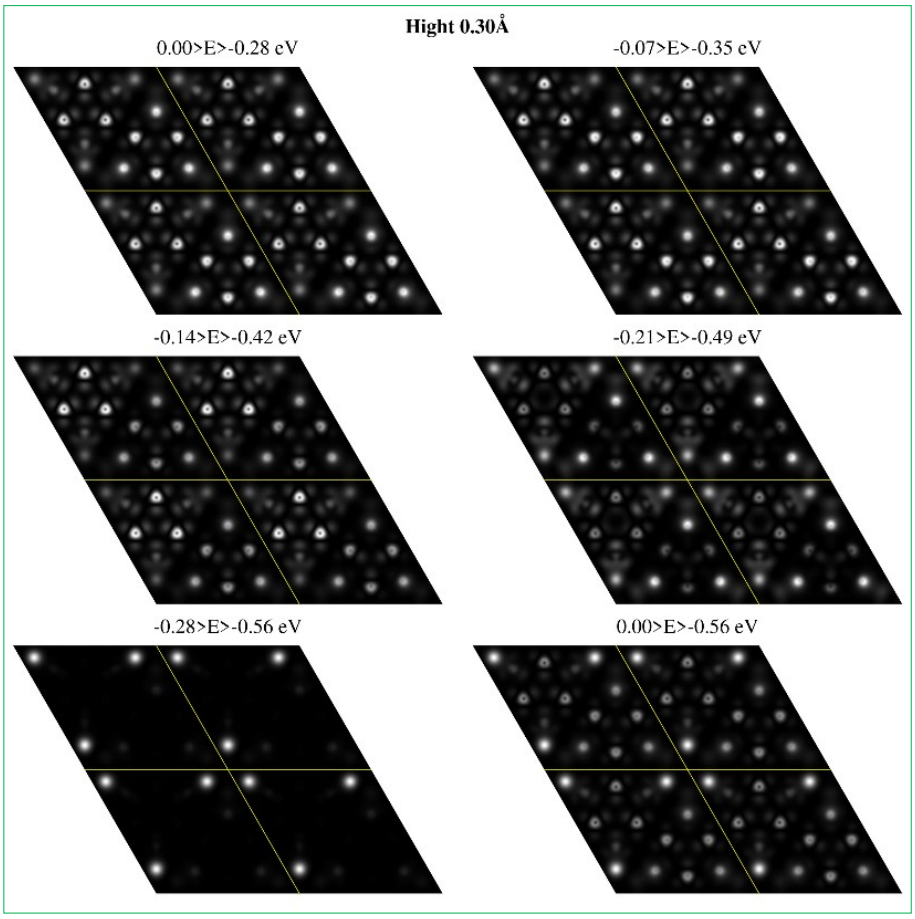


**Fig. S10.** STM of DAS-d8-T6H6 at the height of 0.3 Å

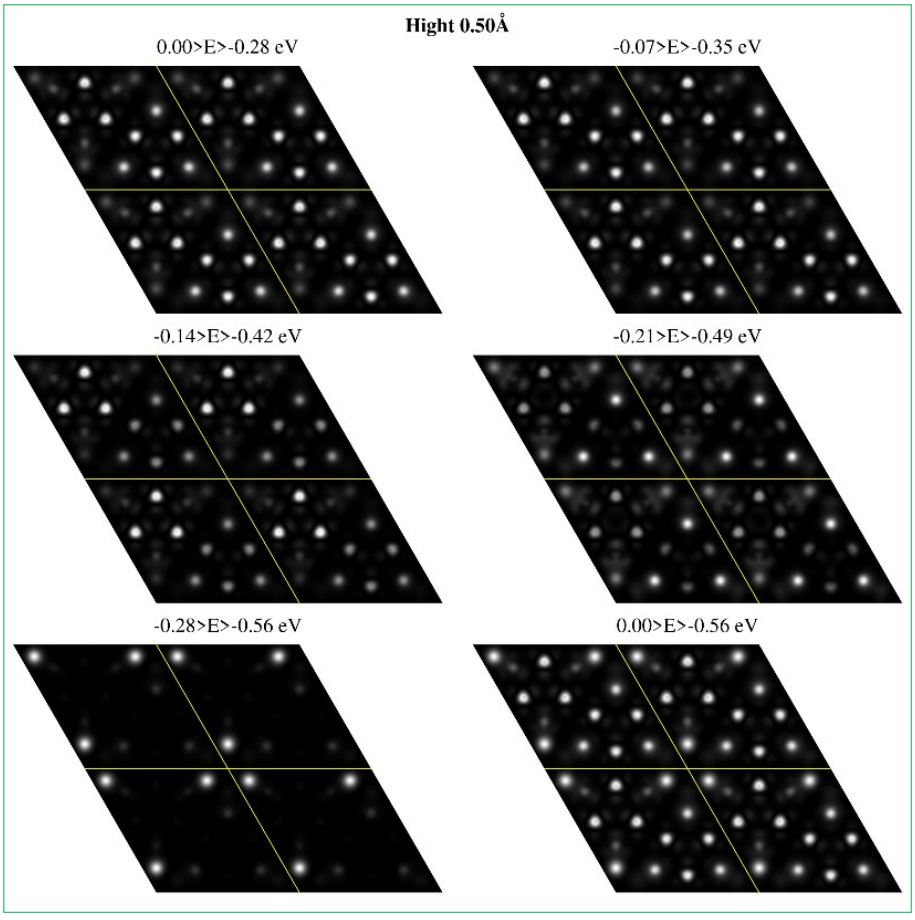


**Fig. S11.** STM of DAS-d8-T6H6 at the height of 0.5 Å

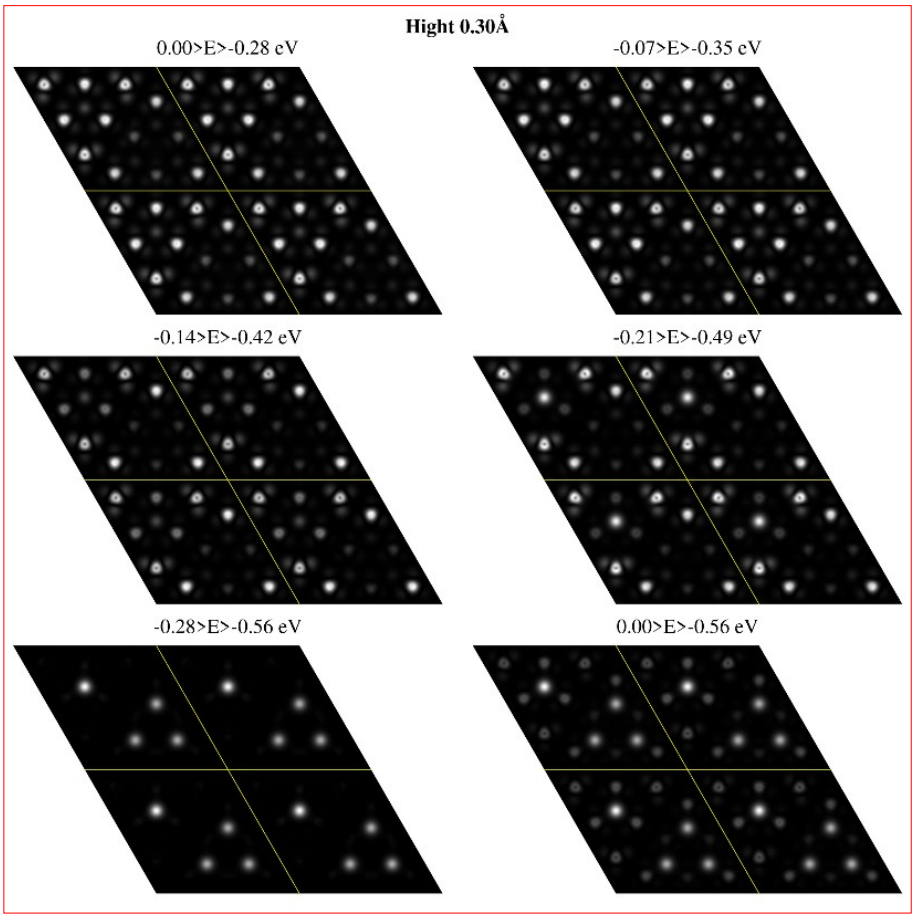


**Fig. S12.** STM of AB-d10-T12 at the height of 0.3 Å

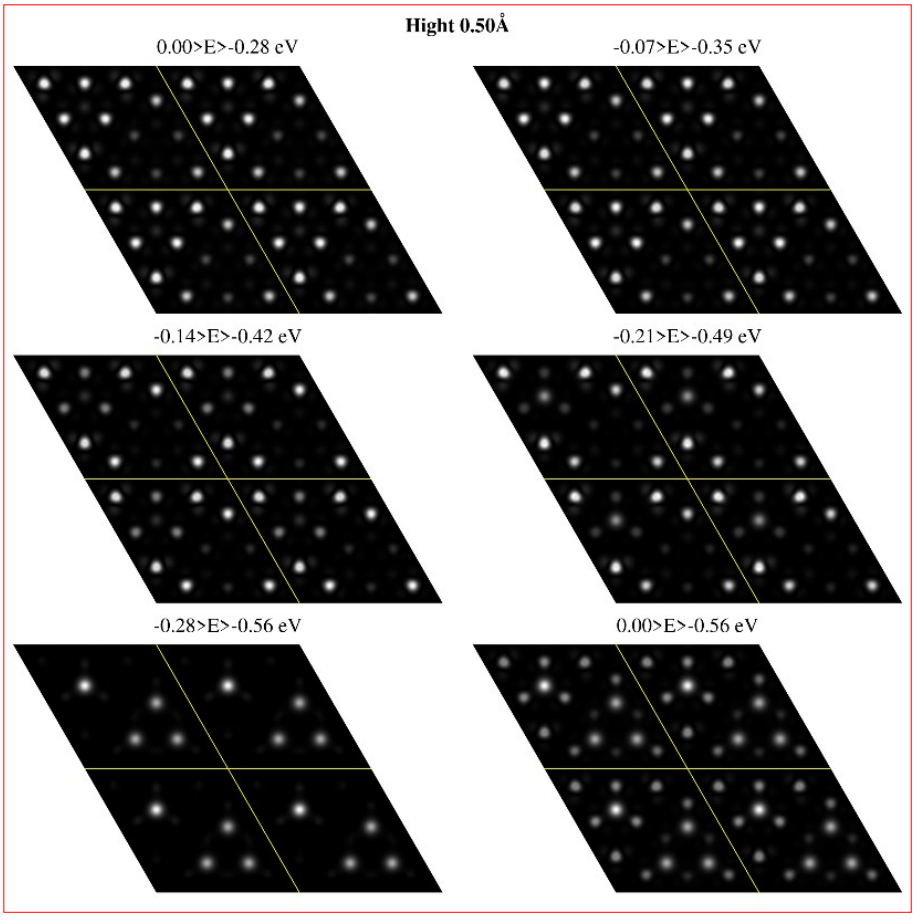


**Fig. S13.** STM of AB-d10-T12 at the height of 0.5Å

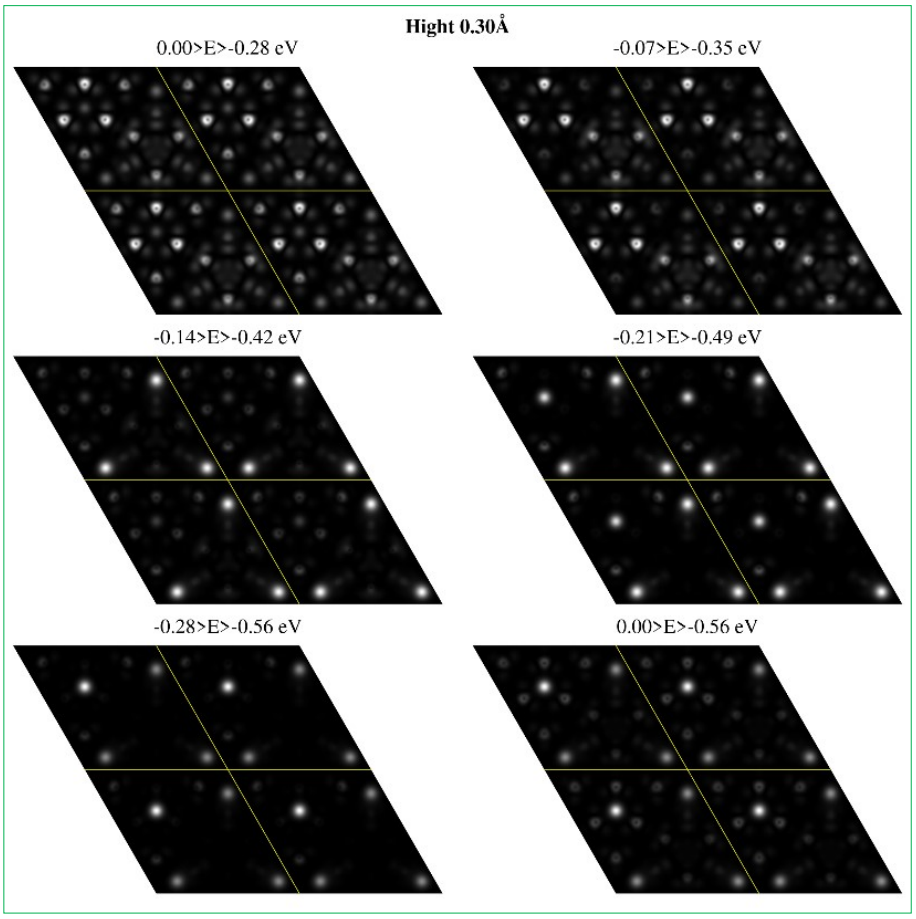


**Fig. S14.** STM of AB-d10-T9H3 at the height of 0.3 Å

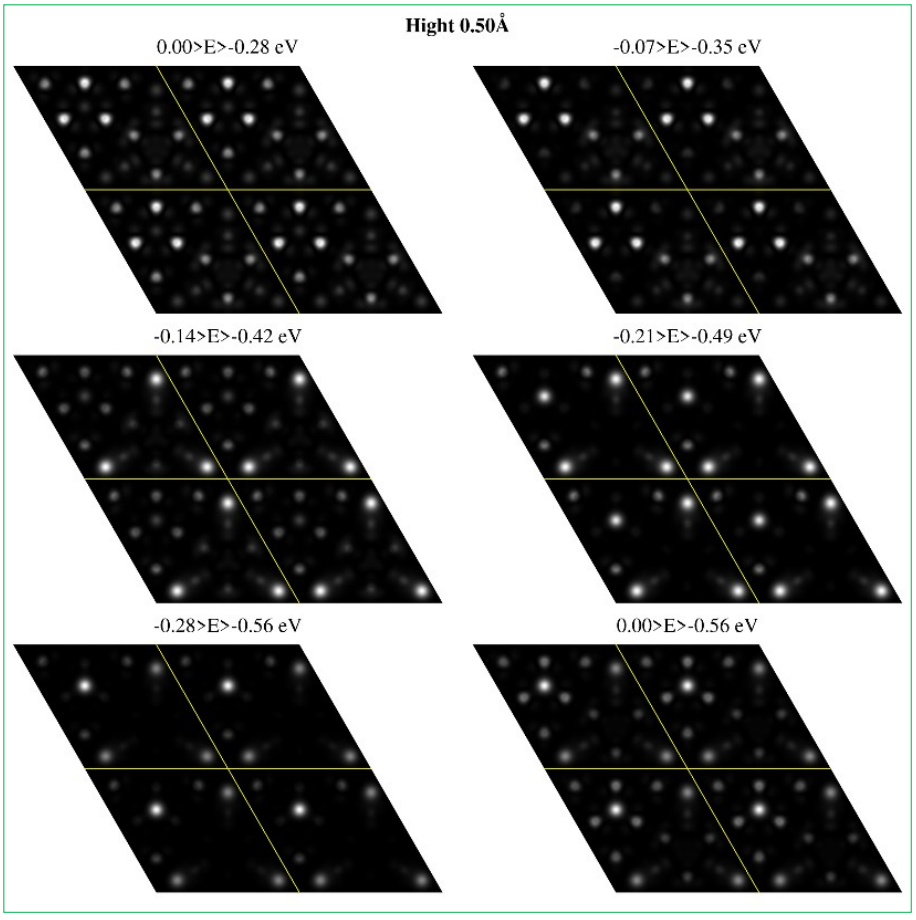


**Fig. S15.** STM of AB-d10-T9H3 at the height of 0.5 Å

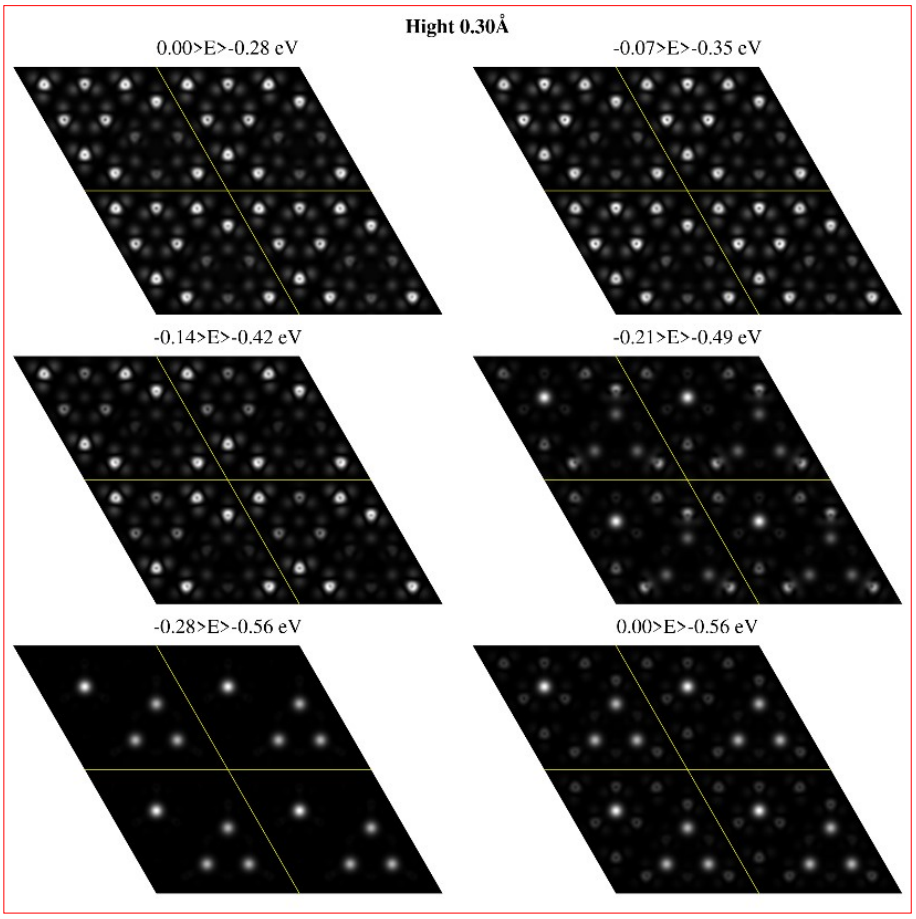


**Fig. S16.** STM of AA-d10-T12 at the height of 0.3 Å

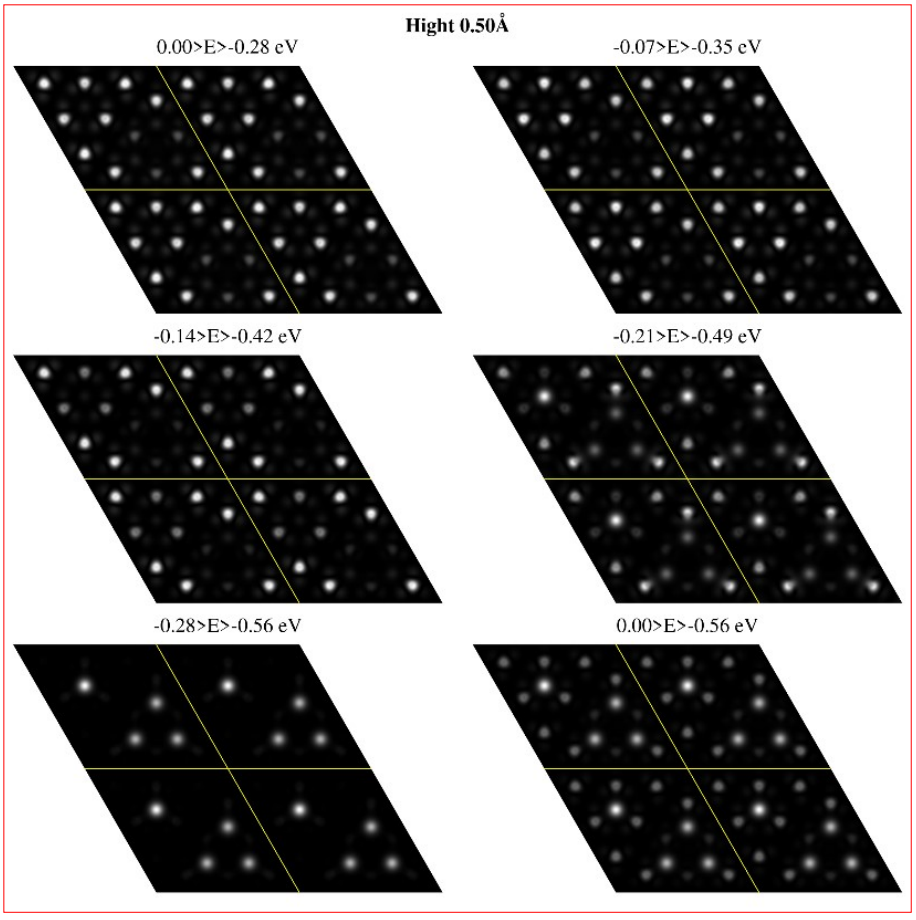


**Fig. S17.** STM of AA-d10-T12 at the height of 0.5 Å

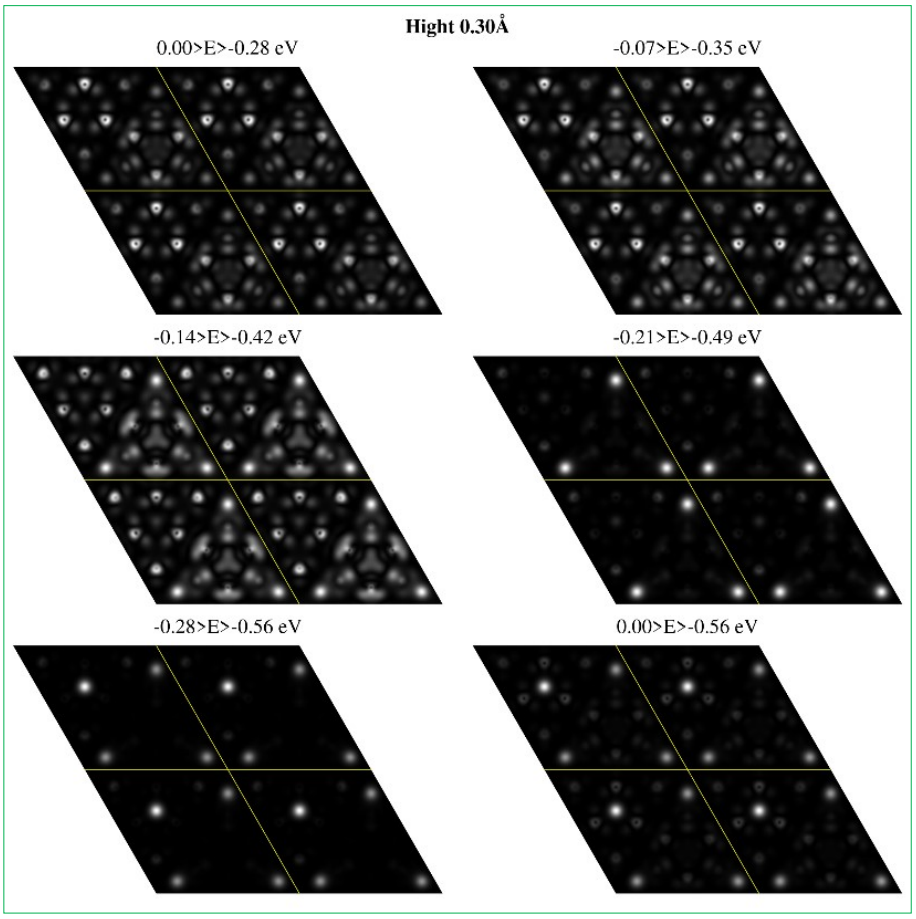


**Fig. S18.** STM of AA-d10-T9H3 at the height of 0.3 Å

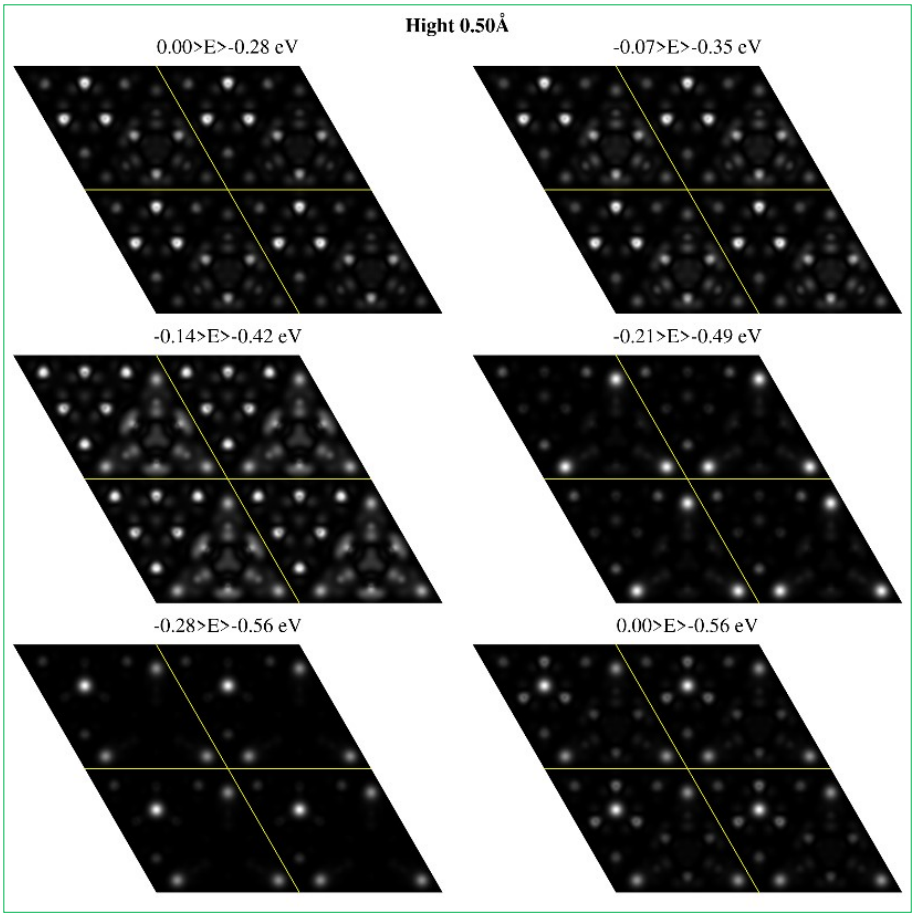


**Fig. S19.** STM of AA-d10-T9H3 at the height of 0.5 Å